

# To be or not to be stable, that is the question: understanding neural networks for inverse problems\*

Davide Evangelista<sup>†</sup>    Elena Loli Piccolomini<sup>‡</sup>    Elena Morotti<sup>§</sup>  
James Nagy<sup>¶</sup>

January 26, 2023

## Abstract

The solution of linear inverse problems arising, for example, in signal and image processing is a challenging problem since the ill-conditioning amplifies the noise on the data. Recently introduced algorithms based on deep learning overwhelm the more traditional model-based approaches, but they typically suffer from instability with respect to data perturbation. In this paper, we theoretically analyze the trade-off between neural networks stability and accuracy in the solution of linear inverse problems. Moreover, we propose different supervised and unsupervised solutions to increase network stability that maintains good accuracy by inheriting, in the network training, regularization from a model-based iterative scheme. Extensive numerical experiments on image deblurring confirm the theoretical results and the effectiveness of the proposed deep learning-based solutions to stably solve noisy inverse problems.

*Keywords*— Neural Networks Stability, Linear Inverse Problems, Deep Learning Algorithms, Image Deblurring

*AMS Subject Classification*— 65K10, 68T07, 68U10

## 1 Introduction

Linear inverse problems of the form:

$$y = Ax^{gt} \tag{1.1}$$

---

\*This work has been partially supported by the GNCS - Gruppo Nazionale per il Calcolo Scientifico [”Apprendimento automatico e tecniche variazionali per la tomografia” INdAM GNCS Project, grant code CUP\_E55F55000270001] and by the U.S. National Science Foundation, grant codes DMS-2038118 and DMS-2208294.

<sup>†</sup>Department of Mathematics, University of Bologna, Italy (davide.evangelista5@unibo.it).

<sup>‡</sup>Department of Computer Science and Engineering, University of Bologna, Italy.

<sup>§</sup>Department of Political and Social Sciences, University of Bologna, Italy.

<sup>¶</sup>Department of Mathematics, Emory University, Atlanta.

where  $A \in \mathbb{R}^{m \times n}$ ,  $m \geq n$ , is a full-rank matrix discretizing a linear operator,  $x^{gt} \in \mathbb{R}^n$  and  $y \in \mathbb{R}^m$ , arise in various image processing applications, such as deblurring, super-resolution or tomographic reconstruction [17, 22]. It is well-known that when (1.1) is the discretization of an ill-posed problem its solution is very challenging when noise affects the data. We consider here the case of data corrupted by Gaussian noise, i.e.

$$y^\delta = Ax^{gt} + e \quad e \sim \mathcal{N}(0, \delta^2 I) \quad (1.2)$$

where  $\delta$  denotes the standard deviation of the white additive Gaussian noise.

Traditional regularization approaches tackle the problem as the minimization of an objective function containing a data-fit term and a regularization prior, with possible further constraints on the solution [5, 10]. They compute accurate solutions, but in general, the computational time required is high and it may be necessary to choose many (input data dependent) parameters.

In the last few years, neural networks have been introduced with great success for the solution of problem (1.2) [2, 20, 7]. Deep learning based algorithms are very fast and do not require parameter setting, but their accuracy is obtained at the expense of stability. Hence, they are not effective in dealing with noisy data. In particular, they often produce poor results when applied to data corrupted by noise different from the one learned in the training phase. This is usually referred to as network instability. Some authors have empirically studied the stability of neural networks for the solution of inverse problems in the compressed sensing framework [13, 29, 30]. Recent studies [8, 14] demonstrate that it is not possible to achieve optimal stability and accuracy at the same time. However, a mathematically grounded understanding is still challenging.

**Contributions** The contributions of this work are the following. First, we adapt the regularization theory, presented by the authors in [9], to the solution of data-driven inverse problems. In particular, Engl et al. analyzed regularization in Hilbert spaces, whereas we consider discrete inverse problems (also studied in [16, 17]) with a focus on deep learning-based algorithms. Second, we analyze the accuracy and stability of neural networks for the solution of ill-posed linear inverse problems, by proving a mathematical relation showing that it is not possible to increase stability without decreasing accuracy. Finally, we propose the following three solutions to improve stability while preserving good accuracy of neural networks for the solution of a discrete inverse problem. The first one is an unsupervised approach, where the targets are the solutions of (1.2) computed by a regularization method. We call this approach REgularized Neural Network (ReNN). The second one is a stabilization of the networks by pre-processing the noisy input data through very few iterations of a regularized iterative algorithm. We call this approach STabilized Neural Network (StNN). Finally, a combination of ReNN and StNN (denoted as StReNN) is also introduced as a good trade-off between stability and accuracy.

**Notations** In order to improve the readability of the work, we briefly describe the notation that is used throughout this paper. In particular, we always consider  $x^{gt}$  to lie on a subset  $\chi$  of  $\mathbb{R}^n$ , the set of admissible data. We assume  $\chi$  to be compact and locally connected since we want that for any admissible datum  $x^{gt} \in \chi$ , there exists a neighborhood  $V$  of  $x^{gt}$  such

that any  $x \in V$  is admissible. We denote as  $\mathcal{Y} = Rg(A; \chi)$  the range of  $A$  over  $\chi$ , where  $A$  is a continuous linear operator. By continuity of  $A$ ,  $\mathcal{Y}$  is compact and locally connected. The compactness of  $\mathcal{Y}$  implies that  $(C^0(\mathcal{Y}, \mathcal{X}), \|\cdot\|_\infty)$  is a Banach space. Thus, when  $f : \mathcal{Y} \rightarrow \mathcal{X}$  is continuous, we assume  $\|f\|$  to be the  $\|\cdot\|_\infty$  norm. On the contrary, when  $x \in \mathcal{X} \subseteq \mathbb{R}^n$  or  $y \in \mathcal{Y} \subseteq \mathbb{R}^m$ , then  $\|x\|$  and  $\|y\|$  will be Euclidian norms. For any  $\epsilon > 0$ , we also define  $\mathcal{Y}^\epsilon = \{y + e; y \in \mathcal{Y}, \|e\| \leq \epsilon\}$ . Since  $\mathcal{Y}^\epsilon$  is compact and locally connected if  $\mathcal{Y}$  is, then also  $(C^0(\mathcal{Y}^\epsilon, \mathcal{X}), \|\cdot\|_\infty)$  is a Banach space and the same discussion we did for  $\mathcal{Y}$  applies.

**Structure of the paper** The paper is organized as follows. In Section 2 we introduce the concept of reconstructor together with the definition of its accuracy and stability; in Section 3, after considering as reconstructors Tikhonov and neural networks, we propose a new regularized reconstructor, named ReNN. A new technique to obtain two stabilized reconstructors, StNN and StReNN, is proposed in Section 4. In Section 5 and Section 6 we describe the experiments performed with the proposed new reconstructors. Finally, in Section 7 we report some conclusions.

## 2 Reconstructors for the solution of linear inverse problems

To solve problem (1.1), we formalize the concept of reconstructor.

**Definition 2.1.** Any continuous function  $\Psi : \mathbb{R}^m \rightarrow \mathbb{R}^n$ , mapping  $y$  to  $x = \Psi(y)$ , is called a reconstructor.

Given a reconstructor  $\Psi$ , we define its accuracy.

**Definition 2.2.** A reconstructor  $\Psi : \mathbb{R}^m \rightarrow \mathbb{R}^n$  is said to be  $\eta^{-1}$ -accurate, with  $\eta > 0$ , if

$$\eta = \sup_{x^{gt} \in \mathcal{X}} \|\Psi(Ax^{gt}) - x^{gt}\|.$$

EXAMPLE 1. An accurate reconstructor of problem 1.1 is given by:

$$\Psi^\dagger(y) = A^\dagger y \tag{2.1}$$

where the  $A^\dagger$  is the pseudo-inverse matrix. In this case  $\Psi^\dagger : \mathbb{R}^m \rightarrow \mathbb{R}^n$  is  $\infty$ -accurate. Indeed,

$$\|\Psi^\dagger(Ax^{gt}) - x^{gt}\| = \|(A^T A)^{-1} A^T (Ax^{gt}) - x^{gt}\| = \|(A^T A)^{-1} (A^T A) x^{gt} - x^{gt}\| = 0.$$

However, reconstructors are rarely applied to noise-free data, hence a focus on the robustness of reconstructors is necessary.

**Definition 2.3.** Let  $\epsilon > 0$  and  $\Psi$  be an  $\eta^{-1}$ -accurate reconstructor applied to problem (1.2). We define the  $\epsilon$ -stability constant  $C_\Psi^\epsilon$  of  $\Psi$  as

$$C_\Psi^\epsilon = \sup_{\substack{x^{gt} \in \mathcal{X} \\ \|e\| \leq \epsilon}} \frac{\|\Psi(Ax^{gt} + e) - x^{gt}\| - \eta}{\|e\|} \tag{2.2}$$

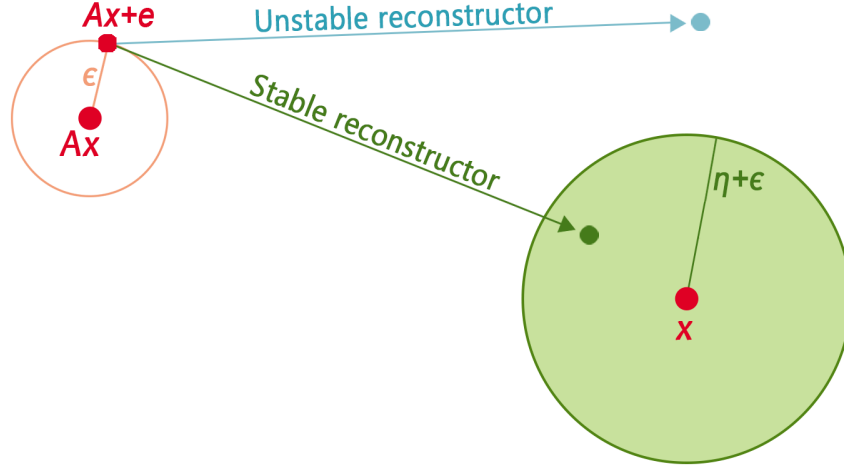


Figure 1: Graphical representation of the  $\epsilon$ -stability for an  $\eta^{-1}$ -accurate reconstructor.

**Definition 2.4.** The reconstructor  $\Psi$  is said to be  $\epsilon$ -stable for a given  $\epsilon$  if  $C_{\Psi}^{\epsilon} \in [0, 1)$ .

An  $\epsilon$ -stable reconstructor  $\Psi$  does not amplify corruptions which have norm less than  $\epsilon$  (as graphically represented in Figure 1), since from (2.2) we derive

$$\|\Psi(Ax^{gt} + e) - x^{gt}\| \leq \eta + C_{\Psi}^{\epsilon} \|e\| \quad \forall x^{gt} \in \mathcal{X}, \forall \|e\| \leq \epsilon.$$

**Definition 2.5.** We define the *stability radius*  $\rho$  of  $\Psi$  as

$$\rho = \sup\{\epsilon > 0; C_{\Psi}^{\epsilon} \in [0, 1)\} \quad (2.3)$$

**EXAMPLE 2.** A reconstructor with an infinite stability radius is the following. Given  $\epsilon > 0$ , if  $\mu$  is a probability distribution over  $\mathcal{X}$  (for example,  $\mu$  is the normalized Lebesgue distribution over  $\mathcal{X}$ ), the reconstructor defined as

$$\Psi^{\mathcal{X}, \epsilon}(y^{\delta}) = \int_{\mathcal{X}} x \mu(dx) \quad \forall y^{\delta} \in \mathcal{Y}^{\epsilon}$$

is  $\epsilon$ -stable independently from the value of  $\epsilon > 0$ . Indeed,

$$\|\Psi^{\mathcal{X}, \epsilon}(Ax^{gt} + e) - x^{gt}\| = \left\| \int_{\mathcal{X}} x \mu(dx) - x^{gt} \right\| \leq \rho(\mathcal{X})$$

where  $\rho(\mathcal{X})$  is the radius of  $\mathcal{X}$ , defined as  $\rho(\mathcal{X}) = \inf\{r > 0 : \mathcal{X} \subseteq \mathcal{B}(\int_{\mathcal{X}} x \mu(dx); r)\}$ . As a consequence, the stability constant is zero regardless  $\epsilon$  and  $\Psi^{\mathcal{X}(y), \epsilon}$  has accuracy  $\rho(\mathcal{X})^{-1}$ .

**EXAMPLE 3.** The pseudo-inverse reconstructor  $\Psi^{\dagger}(y)$  in Equation (2.1) is unstable for any  $\epsilon > 0$  when  $A$  is ill-conditioned. Indeed,

$$\|\Psi^{\dagger}(Ax^{gt} + e) - x^{gt}\| = \|(A^T A)^{-1}(A^T A)x^{gt} + (A^T A)^{-1}A^T e - x^{gt}\| = \|(A^T A)^{-1}A^T e\|.$$

If  $A = U\Sigma V^T$  is the Singular Value Decomposition (SVD) of  $A$ , then

$$(A^T A)^{-1}A^T e = (V\Sigma^2 V^T)^{-1}V\Sigma U^T e = V\Sigma^{-1}U^T e = \sum_{i=1}^n \frac{u_i^T e}{\sigma_i} v_i$$

which implies that  $\|(A^T A)^{-1} A^T e\| \gg \|e\|$  when  $A$  is ill-conditioned. These examples shed light on a possible conflict between accuracy and stability for a given reconstructor  $\Psi$ . In the next paragraphs, we study this relationship.

## 2.1 Accuracy vs. stability trade-off

We can derive a relation between accuracy and stability, becoming particularly interesting when  $A$  is ill-conditioned.

**Lemma 2.1.** Let  $\Psi : \mathbb{R}^m \rightarrow \mathbb{R}^n$  be an  $\eta^{-1}$ -accurate reconstructor. Then, for any  $x^{gt} \in \mathcal{X}$  and for any  $\epsilon > 0$ ,  $\exists \tilde{e} \in \mathbb{R}^m$  with  $\|\tilde{e}\| \leq \epsilon$  such that

$$\|\Psi(Ax^{gt} + \tilde{e}) - x^{gt}\| \geq \|A^\dagger \tilde{e}\| - \eta \quad (2.4)$$

*Proof.* Since  $Ax^{gt} \in \mathcal{Y}$  for each  $x^{gt} \in \mathcal{X}$ , and since  $\mathcal{Y}$  is locally connected by assumption, then for any  $\epsilon > 0$  there is an  $\tilde{e} \in \mathbb{R}^m$  with  $\|\tilde{e}\| \leq \epsilon$  such that  $Ax^{gt} + \tilde{e} \in \mathcal{Y}$ . Thus,  $\exists x' \in \mathcal{X}$  such that  $Ax^{gt} + \tilde{e} = Ax'$ . Consequently,

$$\|\Psi(Ax^{gt} + \tilde{e}) - x^{gt}\| = \|\Psi(Ax') - x^{gt}\| \geq \|x' - x^{gt}\| - \|\Psi(Ax') - x'\| \geq \|x' - x^{gt}\| - \eta$$

Since,  $Ax^{gt} + \tilde{e} = Ax'$  by construction, it holds that  $\tilde{e} = A(x^{gt} - x')$ , which implies that  $x^{gt} - x' = A^\dagger \tilde{e}$ . To conclude,

$$\|\Psi(Ax^{gt} + \tilde{e}) - x^{gt}\| \geq \|x' - x^{gt}\| - \eta = \|A^\dagger \tilde{e}\| - \eta$$

■

**Theorem 2.1** (Trade-off Theorem). Under the same assumptions of Lemma 2.1, it holds that

$$C_\Psi^\epsilon \geq \frac{\|A^\dagger \tilde{e}\| - 2\eta}{\|\tilde{e}\|} \quad (2.5)$$

*Proof.* By the definition of  $\epsilon$ -stability constant, if  $\|\tilde{e}\| \leq \epsilon$  is the perturbation defined on Lemma 2.1, we have

$$\begin{aligned} C_\Psi^\epsilon &= \sup_{\substack{x^{gt} \in \mathcal{X} \\ e: \|e\| \leq \epsilon}} \frac{\|\Psi(Ax^{gt} + e) - x^{gt}\| - \eta}{\|e\|} \geq \sup_{x^{gt} \in \mathcal{X}} \frac{\|\Psi(Ax^{gt} + \tilde{e}) - x^{gt}\| - \eta}{\|\tilde{e}\|} \geq \\ &\geq \sup_{x^{gt} \in \mathcal{X}} \frac{\|A^\dagger \tilde{e}\| - 2\eta}{\|\tilde{e}\|} = \frac{\|A^\dagger \tilde{e}\| - 2\eta}{\|\tilde{e}\|}. \end{aligned}$$

■

**Corollary 2.1.** Given the assumptions of Theorem 2.1, if  $\mathcal{X} = \mathbb{R}^n$ , there is a constant  $C(A) > 0$  which depends only on  $A$ , such that

$$\rho \leq \frac{2}{\eta^{-1} C(A)}. \quad (2.6)$$

*Proof.* Consider a reconstructor  $\Psi$ . By Theorem 2.1, for a given  $\epsilon > 0$ , if

$$\frac{\|A^\dagger e\| - 2\eta}{\|\tilde{e}\|} \geq 1,$$

then  $C_\Psi^\epsilon \geq 1$  and  $\Psi$  is unstable. Let  $e \in \mathbb{R}^m$  with  $\|e\| \leq \epsilon$  be fixed and let  $A = U\Sigma V^T$  be the SVD decomposition of  $A$ . Let  $k$  is the biggest integer such that the projection of  $e$  over the space generated by  $u_k$ , the  $k$ -th column of  $U$ , is non-zero. For simplicity, assume  $e = \|e\|u_k$ . Note that

$$A^\dagger e = V\Sigma^{-1}U^T e = \sum_{i=1}^n \frac{u_i^T e}{\sigma_i} v_i = \frac{u_k^T e}{\sigma_k} v_k = \frac{\|e\|}{\sigma_k} v_k.$$

Consequently,  $\|A^\dagger e\| = \frac{\|e\|}{\sigma_k}$ , which implies that

$$\|A^\dagger e\| - \|e\| = \frac{1 - \sigma_k}{\sigma_k} \|e\| \geq \underbrace{\frac{1 - \sigma_n}{\sigma_n}}_{C(A)} \|e\|.$$

To conclude, note that if

$$\|e\| \geq \frac{2\eta}{C(A)}$$

then

$$\|A^\dagger e\| - \|e\| \geq C(A)\|e\| \geq 2\eta \iff \frac{\|A^\dagger e\| - 2\eta}{\|e\|} \geq 1$$

which implies that  $\Psi$  is unstable. Thus,

$$\rho \leq \frac{2}{\eta^{-1}C(A)}.$$

■

The relation (2.6) between the stability radius  $\rho$  and the accuracy  $\eta^{-1}$  suggests that there exists a trade-off between accuracy and stability, showing that a very accurate reconstructor is unstable for noise corruption larger than  $\frac{2}{\eta^{-1}C(A)}$ . We remark that for ill-conditioned problems  $C(A) = \frac{1-\sigma_n}{\sigma_n}$  can be very large.

## 2.2 A sufficient condition for stability

Whenever the reconstructor is (locally) Lipschitz continuous, we can also derive conditions assessing stability. First of all, we recall the definition of locally Lipschitz continuous reconstructors.

**Definition 2.6.** Given  $\mathcal{Y} \subseteq \mathbb{R}^m$  and  $\epsilon > 0$ , we define the  $\epsilon$ -Lipschitz (also called local Lipschitz) constant of  $\Psi$  over  $\mathcal{Y}$  as:

$$L^\epsilon(\Psi, \mathcal{Y}) = \sup_{\substack{y \in \mathcal{Y}, z \in \mathbb{R}^m \\ \|z - y\| \leq \epsilon}} \frac{\|\Psi(z) - \Psi(y)\|}{\|z - y\|} \quad (2.7)$$

If  $L^\epsilon(\Psi, \mathcal{Y}) < \infty$  for some  $\epsilon > 0$ , then  $\Psi$  is said to be locally Lipschitz continuous.

Focusing on our problem (1.2), we are interested in the cases where  $\mathcal{Y} = Rg(A, \mathcal{X})$ . In this case,  $y \in \mathcal{Y}$  implies that  $\exists x^{gt} \in \mathcal{X}$  such that  $y = Ax^{gt}$  and each  $z \in \mathbb{R}^m$  with  $\|z - y\| \leq \epsilon$  can be characterized by  $z = Ax^{gt} + e$  for some  $e \in \mathbb{R}^m$  with  $\|e\| \leq \epsilon$ . Thus, the definition of  $L^\epsilon(\Psi, \mathcal{Y})$  can be rewritten as:

$$L^\epsilon(\Psi, \mathcal{Y}) = \sup_{\substack{x^{gt} \in \mathcal{X} \\ \|e\| \leq \epsilon}} \frac{\|\Psi(Ax^{gt} + e) - \Psi(Ax^{gt})\|}{\|e\|}.$$

From now on, we always assume  $\mathcal{Y} = Rg(A, \mathcal{X})$ .

The importance of the local Lipschitz constant  $L^\epsilon(\Psi, \mathcal{Y})$  lies in its strong relationship to the stability constant  $C_\Psi^\epsilon$  of the reconstructor. Indeed, if  $y = Ax^{gt} \in \mathcal{Y}$  is corrupted by additional noise  $e$  with  $\|e\| \leq \epsilon$ , then  $L^\epsilon(\Psi, \mathcal{Y})$  represents the maximum variation of the reconstruction via  $\Psi$  around the corrupted  $y$ . The following Proposition confirms this point.

**Proposition 2.1.** Let  $\Psi : \mathbb{R}^m \rightarrow \mathbb{R}^n$  be a reconstructor with accuracy  $\eta^{-1} > 0$  and local Lipschitz constant  $L^\epsilon(\Psi, \mathcal{Y})$ . Then, given  $\|e\| \leq \epsilon$ , it holds:

$$\|\Psi(Ax^{gt} + e) - x^{gt}\| \leq \eta + L^\epsilon(\Psi, \mathcal{Y})\|e\| \quad (2.8)$$

*Proof.* By the triangle inequality, it follows that

$$\|\Psi(Ax^{gt} + e) - x^{gt}\| \leq \|\Psi(Ax^{gt} + e) - \Psi(Ax^{gt})\| + \|\Psi(Ax^{gt}) - x^{gt}\|.$$

Since  $\|e\| \leq \epsilon$ , the definition of local Lipschitz constant implies that

$$\|\Psi(Ax^{gt} + e) - \Psi(Ax^{gt})\| \leq L^\epsilon(\Psi, \mathcal{Y})\|Ax^{gt} + e - Ax^{gt}\| = L^\epsilon(\Psi, \mathcal{Y})\|e\|,$$

whereas the accuracy of  $\Psi$  gives

$$\|\Psi(Ax^{gt}) - x^{gt}\| \leq \eta.$$

Thus, we can conclude

$$\|\Psi(Ax^{gt} + e) - x^{gt}\| \leq L^\epsilon(\Psi, \mathcal{Y})\|e\| + \eta.$$

■

**Corollary 2.2.** Under the assumptions of Proposition 2.1,

$$C_{\Psi}^{\epsilon} \leq L^{\epsilon}(\Psi, \mathcal{Y}) \quad (2.9)$$

*Proof.* From inequality (2.8), we have

$$\|\Psi(Ax^{gt} + e) - x^{gt}\| \leq \eta + L^{\epsilon}(\Psi, \mathcal{Y})\|e\| \iff L^{\epsilon}(\Psi, \mathcal{Y}) \geq \frac{\|\Psi(Ax^{gt} + e) - x^{gt}\| - \eta}{\|e\|}$$

for any  $x^{gt} \in \mathcal{X}$  and any  $e \in \mathbb{R}^m$  with  $\|e\| \leq \epsilon$ . Consequently,  $L^{\epsilon}(\Psi, \mathcal{Y})$  is a majorant of the set

$$\left\{ \frac{\|\Psi(Ax^{gt} + e) - x^{gt}\| - \eta}{\|e\|}; x^{gt} \in \mathcal{X}, \|e\| \leq \epsilon \right\}.$$

Since  $C_{\Psi}^{\epsilon}$  is defined as the supremum of this set, by the minimality of the supremum we have  $C_{\Psi}^{\epsilon} \leq L^{\epsilon}(\Psi, \mathcal{Y})$ . ■

Corollary 2.2 proves that  $\Psi$  is  $\epsilon$ -stable if  $L^{\epsilon}(\Psi, \mathcal{Y}) < 1$ .

### 3 Neural Networks as reconstructors

In this section, we analyze neural networks as particular reconstructors for problem (1.1). If we suppose a sequence of approximators  $\{\Psi_{\theta}\}$  depending on a vector of parameters  $\theta$  approximating a reconstructor  $\Psi$ , we prove in the following theorem that the stability of  $\Psi_{\theta}$  is strongly related to the stability of  $\Psi$ .

**Theorem 3.1** (Approximation Theorem for Reconstructors). Let  $\Psi$  be an  $\eta^{-1}$ -accurate reconstructor and  $\{\Psi_{\theta}\}_{\theta \in \mathbb{R}^s}$  a set of reconstructors with accuracy  $\eta_{\theta}^{-1}$  for any  $\theta$ . We define, for any  $\theta \in \mathbb{R}^s$ :

$$\Delta(\theta) := \sup_{x^{gt} \in \mathcal{X}} \|\Psi_{\theta}(Ax^{gt}) - \Psi(Ax^{gt})\|$$

and

$$\Delta_{\epsilon}(\theta) := \sup_{y^{\delta} \in \mathcal{Y}^{\epsilon}} \|\Psi_{\theta}(y^{\delta}) - \Psi(y^{\delta})\|$$

If  $\Delta(\theta) \rightarrow 0$  when  $\theta \rightarrow \theta^*$ , then:

$$\lim_{\Delta(\theta) \rightarrow 0} \eta_{\theta} = \eta. \quad (3.1)$$

Moreover, if  $\Delta_{\epsilon}(\theta) \rightarrow 0$  when  $\theta \rightarrow \theta_{\epsilon}^*$ , then:

$$\lim_{\Delta_{\epsilon}(\theta) \rightarrow 0} C_{\Psi_{\theta}}^{\epsilon} = C_{\Psi}^{\epsilon}. \quad (3.2)$$

*Proof.* Consider  $x^{gt} \in \mathcal{X}$ . Since

$$\|\Psi_{\theta}(Ax^{gt}) - x^{gt}\| \leq \|\Psi(Ax^{gt}) - x^{gt}\| + \|\Psi_{\theta}(Ax^{gt}) - \Psi(Ax^{gt})\|$$

and

$$\|\Psi_{\theta}(Ax^{gt}) - x^{gt}\| \geq \|\Psi(Ax^{gt}) - x^{gt}\| - \|\Psi_{\theta}(Ax^{gt}) - \Psi(Ax^{gt})\|$$

it holds that:

$$| \|\Psi_\theta(Ax^{gt}) - x^{gt}\| - \|\Psi(Ax^{gt}) - x^{gt}\| | \leq \|\Psi_\theta(Ax^{gt}) - \Psi(Ax^{gt})\| \leq \Delta(\theta)$$

which implies that  $\|\Psi_\theta(Ax^{gt}) - x^{gt}\| \rightarrow \|\Psi(Ax^{gt}) - x^{gt}\|$  as  $\Delta(\theta) \rightarrow 0$  and consequently,  $\eta_\theta \rightarrow \eta$  as  $\Delta(\theta) \rightarrow 0$ .

Now, consider  $\epsilon > 0$  and  $e \in \mathbb{R}^m$  with  $\|e\| \leq \epsilon$ . Following the computation above, it holds

$$| \|\Psi_\theta(Ax^{gt} + e) - x^{gt}\| - \|\Psi(Ax^{gt} + e) - x^{gt}\| | \leq \Delta_\epsilon(\theta)$$

which implies that  $\|\Psi_\theta(Ax^{gt} + e) - x^{gt}\| \rightarrow \|\Psi(Ax^{gt} + e) - x^{gt}\|$  for  $\Delta_\epsilon(\theta) \rightarrow 0$ . Consequently, for  $\Delta_\epsilon(\theta) \rightarrow 0$ ,

$$C_{\Psi_\theta}^\epsilon = \sup_{\substack{x^{gt} \in \mathcal{X} \\ \|e\| \leq \epsilon}} \frac{\|\Psi_\theta(Ax^{gt} + e) - x^{gt}\| - \eta_\theta}{\|e\|} \rightarrow \sup_{\substack{x^{gt} \in \mathcal{X} \\ \|e\| \leq \epsilon}} \frac{\|\Psi(Ax^{gt} + e) - x^{gt}\| - \eta}{\|e\|} = C_\Psi^\epsilon$$

which concludes the proof. ■

**Corollary 3.1.** For any  $\theta \in \mathbb{R}^s$ , it holds:

$$\eta_\theta \leq \eta + \Delta(\theta) \tag{3.3}$$

*Proof.* Consider  $x^{gt} \in \mathcal{X}$ . Then

$$\|\Psi_\theta(Ax^{gt}) - x^{gt}\| \leq \|\Psi_\theta(Ax^{gt}) - \Psi(Ax^{gt})\| + \|\Psi(Ax^{gt}) - x^{gt}\|$$

since  $\|\Psi_\theta(Ax^{gt}) - \Psi(Ax^{gt})\| \leq \Delta(\theta)$  by hypothesis, while  $\|\Psi(Ax^{gt}) - x^{gt}\| \leq \eta$  since  $\Psi$  is  $\eta^{-1}$ -accurate, then

$$\|\Psi_\theta(Ax^{gt}) - x^{gt}\| \leq \eta + \Delta(\theta)$$

which shows that  $\eta_\theta \leq \eta + \Delta(\theta)$ . ■

In the following, we will consider as family  $\{\Psi_\theta\}_{\theta \in \mathbb{R}^s}$  the neural networks.

**Definition 3.1.** Given a neural network architecture  $\mathcal{A} = (\nu, S)$  where  $\nu = (\nu_0, \nu_1, \dots, \nu_L) \in \mathbb{N}^{L+1}$ ,  $\nu_0 = m, \nu_L = n$ , defines the width of each layer and  $S = (S_{1,1}, \dots, S_{L,L}), S_{j,k} \in \mathbb{R}^{\nu_j \times \nu_k}$  is the set of matrices representing the skip connections, we define the parametric family of neural network reconstructors with architecture  $\mathcal{A}$ , parameterized by  $\theta \in \mathbb{R}^s$ , as

$$\mathcal{F}_\theta^{\mathcal{A}} = \{\Psi_\theta : \mathbb{R}^m \rightarrow \mathbb{R}^n; \theta \in \mathbb{R}^s\}$$

where  $\Psi_\theta(y^\delta) = z^L$  is given by:

$$\begin{cases} z^0 = y \\ z^{l+1} = \rho(W^l z^l + b^l + \sum_{k=1}^l S_{l,k} z^k) \quad \forall l = 0, \dots, L-1 \end{cases} \tag{3.4}$$

and  $W^l \in \mathbb{R}^{\nu_{l+1} \times \nu_l}$  is the weight matrix,  $b^l \in \mathbb{R}^{\nu_{l+1}}$  is the bias vector.

Given  $\mathcal{S} \subseteq \mathcal{X}$ , consider the dataset  $\mathbb{D} = \{(y_i^\delta, x_i^{gt}); x_i^{gt} \in \mathcal{S}\}_{i=1}^{N_{\mathbb{D}}}$  of images such that, for any  $i = 1, \dots, N_{\mathbb{D}}$ ,  $y_i^\delta = Ax_i^{gt} + e_i$ ,  $e_i \sim \mathcal{N}(0, \delta^2 I)$ . Training a neural network to solve the inverse problem (1.2) means to compute the reconstructor  $\Psi_\theta \in \mathcal{F}_\theta^A$  solving the minimization problem:

$$\min_{\Psi_\theta \in \mathcal{F}_\theta^A} \frac{1}{N_{\mathbb{D}}} \sum_{i=1}^{N_{\mathbb{D}}} \ell(\Psi_\theta(y_i^\delta), x_i^{gt}) \quad (3.5)$$

where  $\ell : \mathbb{R}^n \times \mathbb{R}^n \rightarrow \mathbb{R}_+$  is the loss function. If we choose as loss function the Mean Squared Error (MSE), (3.5) is equivalent to:

$$\min_{\Psi_\theta \in \mathcal{F}_\theta^A} \sum_{i=1}^{N_{\mathbb{D}}} \|\Psi_\theta(y_i^\delta) - x_i^{gt}\|_2^2 = \min_{\Psi_\theta \in \mathcal{F}_\theta^A} \sum_{i=1}^{N_{\mathbb{D}}} \|\Psi_\theta(y_i^\delta) - \Psi^\dagger(Ax_i^{gt})\|_2^2 \quad (3.6)$$

which results equivalent to minimize the error  $\Delta(\theta)$  introduced in Theorem 3.1 with  $\Psi = \Psi^\dagger$ . Hence, since  $\Psi^\dagger$  is  $\infty$ -accurate, the limit in Equation (3.1) is equal to zero. As a consequence of Theorem 2.1, when  $A$  is ill-conditioned it holds:

$$C_{\Psi_\theta}^\epsilon \approx \frac{\|A^\dagger \tilde{e}\|}{\|\tilde{e}\|} \gg 1.$$

This confirms that an effective training produces a very accurate but unstable reconstructor  $\Psi_\theta$ . Recently, more than one approach has been proposed for stabilization.

A common technique to improve robustness in neural networks is to modify the loss function  $\ell$  to enforce consistency, as developed in [15, 19]. The idea is to define  $\Psi_\theta$  such as

$$\Psi_\theta(y^\delta) \in \arg \min_{x \in \mathbb{R}^n} \frac{1}{2} \|Ax - y^\delta\|^2. \quad (3.7)$$

Unfortunately, it has been proved that this approach does not fully solve instabilities [14]. Another common approach to reduce instabilities in neural networks is adversarial training [31], which can be implemented by data augmentation [24, 12]. The idea is to use equivariant transformations of  $A$  to generate new data. Unfortunately, for ill-conditioned matrices, enlarging the dataset potentially increases instability [14].

A third approach, called noise injection, consists in adding noise to the input of the network during training. It has been proved in [6] that this is equivalent to adding Tikhonov regularization to the loss function. Even if, as explained in [3], this technique improves the stability of the resulting network, however, it is not clear to which extent the accuracy of the resulting model is affected by noise injection and, moreover, how much noise should be added to any input to maximize the trade-off between stability and accuracy.

In the following, we propose new approaches to stabilize accurate neural networks as solvers of (1.2).

### 3.1 Better conditioning implies better reconstructors: the ReNN approach

To introduce our proposal, we first consider Tikhonov method, representing a stable reconstructor [27, 28] defined as:

$$\Psi^{\lambda, L}(y^\delta) = \arg \min_{x \in \mathbb{R}^n} \frac{1}{2} \|Ax - y^\delta\|^2 + \frac{\lambda}{2} \|Lx\|^2 \quad (3.8)$$

where  $\lambda > 0$  is the regularization parameter and  $L \in \mathbb{R}^{d \times n}$  is a matrix such that  $\ker(A) \cap \ker(L) = \{0\}$ .  $L$  is usually chosen to be the identity or the forward-difference operator. We can prove the following proposition.

**Proposition 3.1.** Let  $\epsilon > 0$  and  $L \in \mathbb{R}^{d \times n}$ . Then  $\exists \lambda > 0$  such that

$$C_{\Psi^{\lambda,L}}^\epsilon \leq L^\epsilon(\Psi^{\lambda,L}, \mathcal{Y}) < 1 \quad (3.9)$$

*Proof.* For any  $\lambda > 0$  and any  $y^\delta \in \mathcal{Y}^\epsilon$ , it can be show, by considering the normal equations of (3.8), that

$$\Psi^{\lambda,L}(y^\delta) = \frac{1}{\lambda} \left( \frac{1}{\lambda} A^T A + L^T L \right)^{-1} A^T y^\delta$$

Consequently, for any  $y^\delta \in \mathcal{Y}^\epsilon$ , it holds that  $\Psi^{\lambda,L}(y^\delta) \rightarrow 0$  for  $\lambda \rightarrow \infty$ . Then

$$L^\epsilon(\Psi^{\lambda,L}, \mathcal{Y}) = \sup_{\substack{x^{gt} \in \mathcal{X} \\ \|e\| \leq \epsilon}} \frac{\|\Psi^{\lambda,L}(Ax^{gt} + e) - \Psi^{\lambda,L}(Ax^{gt})\|}{\|e\|} \rightarrow 0 \quad \text{for } \lambda \rightarrow \infty$$

Which implies that for all  $\alpha > 0$ , there exists  $\bar{\lambda} > 0$  such that for any  $\lambda > \bar{\lambda}$ ,  $L^\epsilon(\Psi^{\lambda,L}, \mathcal{Y}) < \alpha$ . Choosing  $\alpha = 1$  gives the required result. ■

Now, we can improve neural network stability by re-defining the training of neural networks, forcing the convergence of  $\Psi_\theta$  towards Tikhonov regularized reconstructor  $\Psi^{\lambda,L}$ , which is  $\epsilon$ -stable for a suitable value of  $\lambda$ .

To this aim, we train the neural network by computing:

$$\min_{\Psi_\theta \in \mathcal{F}_\theta^A} \sum_{i=1}^{N_D} \|\Psi_\theta(y_i^\delta) - \Psi^{\lambda,L}(y_i^\delta)\|_2^2, \quad (3.10)$$

which corresponds to the minimization of  $\Delta_\epsilon(\theta)$  in Theorem 3.1. Since  $C_{\Psi^{\lambda,L}}^\epsilon < 1$  for suitable values of  $\lambda > 0$  (see Proposition (3.1)), the limit in Equation (3.2) (with  $\Psi = \Psi^{\lambda,L}$ ) is less than one. Hence, in this case, an effective training should produce an accurate and stable reconstructor  $\Psi_\theta$ .

We will refer to such a network as the Regularized Neural Network (ReNN) and we will indicate it as  $\Psi_\theta^{\lambda,L}$ . The pseudocode to compute  $\Psi_\theta^{\lambda,L}$  is given in Algorithm 1.

## 4 Stabilizers

In this section we propose a further stabilization of neural networks by defining the concept of stabilizer. From the Universal Approximation Theorem [25, 4] we infer that  $\Delta(\theta)$  strongly influences the assessment of the  $\Psi_\theta^{\lambda,L}$  stability which is in fact not guaranteed in case of large values of  $\Delta$ . At the same time we observe that for any  $\Delta(\theta) > 0$  there always exists a neural network  $\Psi_\theta \in \mathcal{F}_\theta^A$  (with suitable  $\mathcal{A}$ ), such that  $\|\Psi_\theta^{\lambda,L} - \Psi^{\lambda,L}\| \leq \Delta(\theta)$ . However, obtaining

**Algorithm 1** Regularized Neural Network (ReNN)

---

**input** a collection  $\{x_i^{gt}\}_{i=1}^{N_{\mathbb{D}}} \subseteq \mathcal{X}$  of data points,  $A \in \mathbb{R}^{m \times n}$  and  $\Psi^{\lambda,L}, \mathcal{A}$   
**for**  $i \leftarrow 1 : N_{\mathbb{D}}$  **do**  
  Compute  $y_i^{\delta} \leftarrow Ax_i^{gt} + e$   
  Compute  $\Psi^{\lambda,L}(y_i^{\delta})$   
  Append  $(y_i^{\delta}, \Psi^{\lambda,L}(y_i^{\delta}))$  to  $\mathbb{D}^{\lambda,L}$   
**end for**  
**Find**

$$\arg \min_{\Psi_{\theta} \in \mathcal{F}_{\theta}^A} \sum_{i=1}^{N_{\mathbb{D}}} \|\Psi_{\theta}(y_i^{\delta}) - \Psi^{\lambda,L}(y_i^{\delta})\|_2^2$$

**return** a trained ReNN  $\Psi_{\theta}$

---

such a neural network can be infeasible in practice, because of the theory-practice gap of numerical computations, as observed in [8, 1]. It becomes therefore necessary to design a new reconstructor, directly facing the stability issue more than the approximation task. To this aim, we now introduce a stabilization strategy.

**Definition 4.1.** A continuous functions  $\phi : \mathbb{R}^m \rightarrow \mathbb{R}^t$  is an  $\epsilon$ -stabilizer of a reconstructor  $\Psi : \mathbb{R}^m \rightarrow \mathbb{R}^n$  if:

1.  $\forall e \in \mathbb{R}^m$  with  $\|e\| \leq \epsilon$ ,  $\exists C_{\phi}^{\epsilon} \in [0, 1)$  and  $\exists e' \in \mathbb{R}^n$  with  $\|e'\| = C_{\phi}^{\epsilon} \|e\|$  such that

$$\phi(Ax + e) = \phi(Ax) + e'. \quad (4.1)$$

2.  $\exists \gamma : \mathbb{R}^t \rightarrow \mathbb{R}^n$  such that  $\Psi = \gamma \circ \phi$ .

In this case, the reconstructor  $\Psi$  is said to be  $\epsilon$ -stabilized. The smallest constant  $C_{\phi}^{\epsilon}$  for which the definition holds is the stability constant of the stabilizer  $\phi$ .

Note that, in the definition of  $\epsilon$ -stabilizer, we are requiring for  $\phi$  only a stability condition as in (4.1) and we do not ask anything about its accuracy. We also remark that, by Definition 4.1, we disentangle the problem of finding an accurate and a stable reconstructor.

Interestingly, given an  $\epsilon$ -stabilized reconstructor  $\Psi = \gamma \circ \phi$ , we can estimate the  $\epsilon$ -stability constant  $C_{\Psi}^{\epsilon}$  of  $\Psi$  by the constant  $C_{\phi}^{\epsilon}$  and the local Lipschitz constant of  $\gamma$  as proved in the following proposition.

**Proposition 4.1.** Let  $\Psi : \mathbb{R}^m \rightarrow \mathbb{R}^n$  be an  $\epsilon$ -stabilized reconstructor,  $\Psi = \gamma \circ \phi$ . If  $C_{\phi}^{\epsilon}$  is the constant defined in (4.1),  $L^{\epsilon}(\gamma, \mathcal{T})$  is the local Lipschitz constant of  $\gamma$  with  $\mathcal{T} = \phi(\mathcal{Y})$ , then

$$C_{\Psi}^{\epsilon} \leq L^{\epsilon}(\gamma, \mathcal{T}) C_{\phi}^{\epsilon}.$$

*Proof.* Let  $x^{gt} \in \mathcal{X}$  and  $\|e\| \leq \epsilon$ . Then,

$$\|\Psi(Ax^{gt} + e) - x^{gt}\| = \|\gamma(\phi(Ax^{gt} + e)) - x^{gt}\|.$$

Since  $\phi$  is a stabilizer,  $\phi(Ax^{gt} + e) = \phi(Ax^{gt}) + e'$  with  $\|e'\| \leq C_\phi^\epsilon \|e\|$ . Thus

$$\begin{aligned} \|(\gamma \circ \phi)(Ax^{gt} + e) - x^{gt}\| &= \|\gamma(\phi(Ax^{gt}) + e') - x^{gt}\| \\ &\leq \|\gamma(\phi(Ax^{gt}) + e') - \gamma(\phi(Ax^{gt}))\| + \|\gamma(\phi(Ax^{gt})) - x^{gt}\| \\ &\leq \eta + L^\epsilon(\gamma, \mathcal{T})\|e'\| \leq \eta + L^\epsilon(\gamma, \mathcal{T})C_\phi^\epsilon \|e\|, \end{aligned}$$

which implies that  $L^\epsilon(\gamma, \mathcal{T})C_\phi^\epsilon$  is a majorant of the set

$$\left\{ \frac{\|\Psi(Ax^{gt} + e) - x^{gt}\| - \eta}{\|e\|}; x^{gt} \in \mathcal{X}, \|e\| \leq \epsilon \right\}.$$

Since  $C_\Psi^\epsilon$  is defined as the supremum of the same set, by the minimality of the supremum we have  $C_\Psi^\epsilon \leq L^\epsilon(\gamma, \mathcal{T})C_\phi^\epsilon$ . ■

Proposition 4.1 implies the following result:

**Theorem 4.1** (Stabilization Condition). For  $\epsilon > 0$ , let  $\phi_1 : \mathbb{R}^m \rightarrow \mathbb{R}^t$  be an  $\epsilon$ -stabilizer of the reconstructor  $\Psi_1 = \gamma_1 \circ \phi_1$  and suppose  $\Psi_2$  be a reconstructor with the same accuracy  $\eta^{-1} > 0$  of  $\Psi_1$ . If

$$C_{\phi_1}^\epsilon \in \left[ 0, \frac{C_{\Psi_2}^\epsilon}{L^\epsilon(\gamma_1, \mathcal{T})} \right] \quad (4.2)$$

then

$$C_{\Psi_1}^\epsilon < C_{\Psi_2}^\epsilon.$$

*Proof.* By hypothesis, both  $\Psi_1 = \gamma_1 \circ \phi_1$  and  $\Psi_2$  are  $\eta^{-1}$ -accurate. Since

$$C_{\phi_1}^\epsilon \in \left[ 0, \frac{C_{\Psi_2}^\epsilon}{L^\epsilon(\gamma_1, \mathcal{T})} \right]$$

and  $C_{\Psi_1}^\epsilon < L^\epsilon(\gamma_1, \mathcal{T})C_{\phi_1}^\epsilon$  by Proposition 4.1, then

$$C_{\Psi_1}^\epsilon \leq L^\epsilon(\gamma_1, \mathcal{T})C_{\phi_1}^\epsilon < L^\epsilon(\gamma_1, \mathcal{T}) \frac{C_{\Psi_2}^\epsilon}{L^\epsilon(\gamma_1, \mathcal{T})} = C_{\Psi_2}^\epsilon$$

which concludes the proof. ■

The introduction of stabilizers opens the possibility of separately designing a stable and accurate reconstructor. In particular, given  $\eta > 0$ , if  $\phi$  is a stabilizer and  $\Psi = \gamma \circ \phi$  is  $\eta^{-1}$ -accurate, then the stability constant of  $\Psi$ ,  $C_\Psi^\epsilon$ , can be decreased by decreasing the stability constant of  $\phi$ , i.e.  $C_\phi^\epsilon$ .

In the next proposition we will show that the accuracy of any  $\epsilon$ -stabilized reconstructor, strongly depends on how far is  $\phi$  from an injective function. Indeed, it holds:

**Proposition 4.2.** Let  $\phi : \mathbb{R}^m \rightarrow \mathbb{R}^t$  be an  $\epsilon$ -stabilizer for an  $\eta^{-1}$ -accurate reconstructor  $\Psi = \gamma \circ \phi$ . Let

$$\sigma(\phi) := \sup\{\|x_1 - x_2\|; x_1, x_2 \in \mathcal{X}, \phi(Ax_1) = \phi(Ax_2)\} \quad (4.3)$$

Then

$$\eta^{-1} \leq \frac{2}{\sigma(\phi)}. \quad (4.4)$$

*Proof.* Let  $x_1, x_2 \in \mathcal{X}$  such that  $\phi(Ax_1) = \phi(Ax_2)$ . Then,

$$\begin{aligned} \|x_1 - x_2\| &\leq \|\phi(Ax_1) - x_1\| + \|\phi(Ax_1) - x_2\| \\ &= \|\phi(Ax_1) - x_1\| + \|\phi(Ax_2) - x_2\| \leq 2\eta \end{aligned}$$

which implies that

$$\eta \geq \frac{\|x_1 - x_2\|}{2}.$$

Since the estimation above holds for any  $x_1, x_2$  with  $\phi(Ax_1) = \phi(Ax_2)$ , then it holds for  $\sigma(\phi)$ , concluding the proof. ■

Note that, if  $\phi$  is the constant reconstructor,  $\sigma(\phi) = \infty$ , which implies that for any  $\gamma$ , the accuracy of  $\Psi = \gamma \circ \phi$  will be zero. Similarly, if  $\sigma(\phi) < \infty$ , then for any  $\eta^{-1} \in (0, \frac{2}{\sigma(\phi)}]$ ,  $\Psi = \gamma \circ \phi$  is  $\eta^{-1}$ -accurate. A flexible way to define such a  $\gamma$ , which is mathematically complex to describe, is to use a neural network.

## 4.1 Iterative algorithm as stabilizers for neural networks

Consider the variational regularized reconstructor  $\Psi^{\lambda, L}$  (3.8). Suppose we compute a sequence of functions  $\{\phi_k\}_{k \in \mathbb{N}}$  approximating  $\Psi^{\lambda, L}$ , i.e. :

$$\lim_{k \rightarrow \infty} \|\phi_k - \Psi^{\lambda, L}\|_{L^2} = 0.$$

A simple way to get it is to consider a convergent iterative algorithm for the solution of (3.8):

$$\begin{cases} x^0 \in \mathbb{R}^n \\ x^{k+1} = \mathcal{T}_k(x^k). \end{cases}$$

Then, for any  $k \in \mathbb{N}$  we can define

$$\phi_k = \circ_{i=1}^k \mathcal{T}_i. \tag{4.5}$$

Clearly, as a consequence of the convergence of the iterates  $\mathcal{T}_k$ ,  $\{\phi_k\}_{k \in \mathbb{N}}$  is a sequence of functions approximating  $\Psi^{\lambda, L}$ . We can now define an  $\epsilon$ -stabilizer by fixing  $K \in \mathbb{N}$  and computing  $\phi_k$  for some  $k \geq K$ .

**Proposition 4.3.** Given a reconstructor  $\Psi : \mathbb{R}^m \rightarrow \mathbb{R}^n$  with local Lipschitz constant  $L^\epsilon(\Psi, \mathcal{Y}) < 1$  and a sequence of functions  $\{\phi_k\}_{k \in \mathbb{N}}$  approximating  $\Psi$ . Then there exists  $K \in \mathbb{N}$  such that for any  $k \geq K$ ,  $\phi_k$  is an  $\epsilon$ -stabilizer.

*Proof.* Consider  $x^{gt} \in X$  and  $e \in \mathbb{R}^m$  with  $\|e\| \leq \epsilon$ . To prove the Theorem, we need to show that for  $k \geq K$ ,

$$\phi_k(Ax^{gt} + e) = \phi_k(Ax^{gt}) + e'$$

with  $\|e'\| = C_\phi^\epsilon \|e\|$  with  $C_\phi^\epsilon \in [0, 1)$ . Let  $e' := \phi_k(Ax^{gt} + e) - \phi_k(Ax^{gt})$ . Then

$$\|e'\| = \|\phi_k(Ax^{gt} + e) - \phi_k(Ax^{gt})\| \leq L^\epsilon(\phi_k, \mathcal{Y}) \|Ax^{gt} + e - Ax^{gt}\| = L^\epsilon(\phi_k, \mathcal{Y}) \|e\|$$

which implies that  $C_{\phi_k}^\epsilon \leq L^\epsilon(\phi_k, \mathcal{Y})$ . Since  $\{\phi_k\}_{k \in \mathbb{N}}$  is a sequence of approximators to  $\Psi$ , then for any  $k \in \mathbb{N}$ , there is a constant  $c_k$  such that  $\|\phi_k(y^\delta) - \Psi(y^\delta)\| \leq c_k$  with  $c_k \rightarrow 0$  as  $k \rightarrow \infty$ . Consequently, it holds

$$\begin{aligned} L^\epsilon(\phi_k, \mathcal{Y}) &= \sup_{\substack{x^{gt} \in \mathcal{X} \\ \|e\| \leq \epsilon}} \frac{\|\phi_k(Ax^{gt} + e) - \phi_k(Ax^{gt})\|}{\|e\|} \\ &\leq \sup_{\substack{x^{gt} \in \mathcal{X} \\ \|e\| \leq \epsilon}} \frac{\|\phi_k(Ax^{gt} + e) - \Psi(Ax^{gt} + e)\| + \|\phi_k(Ax^{gt}) - \Psi(Ax^{gt})\| + \|\Psi(Ax^{gt} + e) - \Psi(Ax^{gt})\|}{\|e\|} \\ &\leq \sup_{\substack{x^{gt} \in \mathcal{X} \\ \|e\| \leq \epsilon}} \frac{\|\Psi(Ax^{gt} + e) - \Psi(Ax^{gt})\| + 2c_k}{\|e\|} \end{aligned}$$

which implies that  $L^\epsilon(\phi_k, \mathcal{Y}) \rightarrow L^\epsilon(\Psi, \mathcal{Y})$  as  $k \rightarrow \infty$ . Since  $L^\epsilon(\Psi, \mathcal{Y}) < 1$ , this implies that  $\exists K \in \mathbb{N}$  such that for any  $k \geq K$ ,  $L^\epsilon(\phi_k, \mathcal{Y}) < 1$ . For those values of  $k$ ,  $C_{\phi_k}^\epsilon \leq L^\epsilon(\phi_k, \mathcal{Y}) < 1$  which implies that  $\phi_k$  is an  $\epsilon$ -stabilizer. ■

Consider the case study of Tikhonov regularized reconstructor  $\Psi^{\lambda, L}$ . We already proved in Proposition 3.1 that  $L^\epsilon(\Psi, \mathcal{Y}) < 1$  for some  $\lambda > 0$ . Moreover, from (3.8) we know that  $\Psi^{\lambda, L}(y^\delta)$ , is the solution of the normal equation system

$$(A^T A + \lambda L^T L)x = A^T y^\delta. \quad (4.6)$$

By Proposition 4.3, the functions  $\phi_k$  chosen as the iterates of an iterative method for the solution of (4.6), such as the Conjugate Gradient for Least Squares (CGLS) [16], defines a stabilizer for a neural network  $\Psi_\theta$ . We can join either NN or ReNN with this stabilizer, obtaining StNN and StReNN, respectively, whose implementation is reported in Algorithms 2 and 3.

Figure 2 schematically represents all the proposed approaches.

---

### Algorithm 2 Stabilized Neural Network (StNN)

---

**input** a collection  $\mathbb{D} = \{(y_i^\delta, x_i^{gt})\}_{i=1}^{N_{\mathbb{D}}}$  of data points, a convergent algorithm  $\mathcal{T}_k$  for  $\Psi^{\lambda, L}$ , an integer  $k \in \mathbb{N}$  such that  $\phi_k$  is an  $\epsilon$ -stabilizer,  $\mathcal{A}$

Find

$$\gamma_\theta = \arg \min_{\gamma_\theta \in \mathcal{F}_\theta^{\mathcal{A}}} \sum_{i=1}^{N_{\mathbb{D}}} \|\gamma_\theta(\phi_k(y_i^\delta)) - x_i^{gt}\|_2^2$$

Define  $\Psi_\theta = \gamma_\theta \circ \phi_k$

**return** a trained StNN  $\Psi_\theta$

---

## 5 Experimental Setup

To assess the theoretical issues proposed, we perform three experiments, denoted as A, B and C in the following.

**Algorithm 3** Stabilized Regularized Neural Network (StReNN)

**input** a collection  $\mathbb{D} = \{(y_i^\delta, x_i^{gt})\}_{i=1}^{N_{\mathbb{D}}}$  of data points, a convergence algorithm  $\mathcal{T}_k$  for  $\Psi^{\lambda,L}$ , an integer  $k \in \mathbb{N}$  such that  $\phi_k$  is an  $\epsilon$ -stabilizer,  $\mathcal{A}$

**for**  $i \leftarrow 1 : N_{\mathbb{D}}$  **do**

    Compute  $y_i^\delta \leftarrow Ax_i^{gt} + e$

    Compute  $\Psi^{\lambda,L}(y_i^\delta)$

    Append  $(y_i^\delta, \Psi^{\lambda,L}(y_i^\delta))$  to  $\mathbb{D}^{\lambda,L}$

**end for**

Find

$$\gamma_\theta = \arg \min_{\gamma_\theta \in \mathcal{F}_\theta^{\mathcal{A}}} \sum_{i=1}^{N_{\mathbb{D}}} \|\gamma_\theta(\phi_k(y_i^\delta)) - x_i^{\lambda,L}\|_2^2$$

Define  $\Psi_\theta = \gamma_\theta \circ \phi_k$

**return** a trained StReNN  $\Psi_\theta$

The codes can be found in our GitHub repository for this work, at [https://github.com/loibo/stabilize\\_neural\\_networks](https://github.com/loibo/stabilize_neural_networks).

As a test case, we consider image deblurring [18], a common inverse problem in imaging. In this case,  $Ax = \mathcal{K} * x$ , where  $\mathcal{K}$  is the blurring kernel and  $*$  denotes convolution. In our experiments, we use the  $11 \times 11$  Gaussian blur kernel:

$$\mathcal{K}_{i,j} = \begin{cases} e^{-\frac{1}{2} \frac{i^2+j^2}{\sigma_G^2}} & i, j \in \{-5, \dots, 5\}^2 \\ 0 & \text{otherwise} \end{cases} \quad (5.1)$$

with variance  $\sigma_G^2 = 1.3$ .

## 5.1 Dataset

Our results have been tested on the famous GoPro image dataset (<https://seungjunh.github.io/Datasets/gopro>), introduced in [23], which is constituted by high-resolution RGB images. All the images have been cropped into patches of size  $256 \times 256$  (without overlapping), converted into grayscale and normalized them in  $[0,1]$ . The images obtained are labelled as  $x_i^{gt}, i = 1, \dots, N$ .

We need two data sets for our experiments:

- $\mathbb{D} = \{(y_i^\delta, x_i^{gt}); y_i^\delta = \mathcal{K} * x_i^{gt} + e_i = Ax_i^{gt} + e_i\}_{i=1}^N$  contains the images representing the blurred and noisy version of  $x_i^{gt}$ , by sampling  $e_i \sim \mathcal{N}(0, \delta^2 \odot I)$ .
- $\mathbb{D}^{\lambda,L} = \{(y_i^\delta, \overline{\Psi^{\lambda,L}(y_i^\delta)})\}_{i=1}^N$  is constituted by the images obtained by applying the Tikhonov reconstructor (3.8) to the corrupted data, using  $L = I$ . In particular, we choose  $\lambda$  heuristically and we computed  $\overline{\Psi^{\lambda,L}(y_i^\delta)}$  by using the CGLS algorithm [16] to solve the normal equations of (3.8).

We split the  $N = 3614$  data samples in  $N_{train} = 2503$  and  $N_{test} = 1111$ .

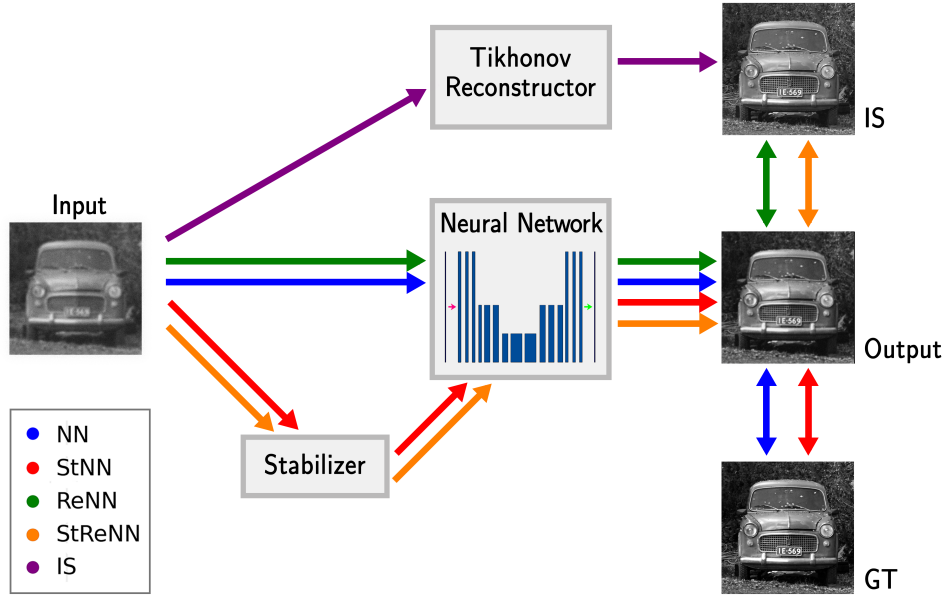


Figure 2: A schematic representation of the proposed methods.

## 5.2 Experiment A

In this first experiment, we trained the networks to solve the noiseless task  $y_i = Ax_i^{gt}$  to perfectly fit the theoretical assumptions. We emphasize that the four proposed models are all based on the same end-to-end U-net architecture, as depicted in Figure 2. For details on the architecture and its training you can refer to [21, 11]. Thus, we trained the neural networks in NN and StNN with the input  $\mathbb{D}$ , and ReNN and StReNN with the input  $\mathbb{D}^{\lambda,L}$ . In StNN and StReNN the input is pre-processed by a stabilizer obtained with  $k = 3$  iterations of the CGLS algorithm applied on (3.8). We remark that by minimizing the MSE either on  $\mathbb{D}$  or  $\mathbb{D}^{\lambda,L}$  we are minimizing  $\Delta(\theta)$  as defined in Theorem 3.1. In order to test the stability of our frameworks with respect to unseen noise on the data, we tested on noisy images  $y_i^\delta = y_i + e_i$  where  $e \sim \mathcal{N}(0, \delta I)$ .

## 5.3 Experiment B

Among the stabilizing solutions listed in Section 3, in this experiment, we tested noise injection, which is considered the most reliable. Hence we modified the training of experiment A by adding Gaussian noise with variance  $\delta^I = 0.025$  to the input of each network. We observe that, concerning StNN and StReNN, the noise has been added after stabilizing the input. Thanks to the improved robustness introduced by noise injection, in this experiment we have tested on noisy images with  $\delta = 0.075$  and  $\delta = 0.105$ .

## 5.4 Experiment C

The last test aims at experimentally checking the results proved in the second part of Theorem 3.1, where in (3.2) we state that, by reducing  $\Delta_\epsilon(\theta)$ , the stability constant  $C_{\Psi_\theta}^\epsilon$  converges

to  $C_{\Psi}^{\epsilon}$ . In this experiment we show that, if we choose  $\Psi$  as the Tikhonov reconstructor we can modify the training of ReNN and StReNN methods to minimize  $\Delta_{\epsilon}(\theta)$  in place of  $\Delta(\theta)$ , aiming at dramatically improving their stability. To do that, we modified the input  $\mathbb{D}^{\lambda,L}$  of the training for ReNN and StReNN by introducing noise in the target, thus obtaining  $\hat{\mathbb{D}}^{\lambda,L} = \{(Ax_i^{gt} + \hat{e}, \Psi^{\lambda,L}(Ax_i^{gt} + \hat{e}))\}_{i=1}^{N_{train}}$  where  $\hat{e} \sim \mathcal{N}(0, \hat{\delta}I)$  with  $\hat{\delta} = 0.025$ .

## 5.5 Results evaluation

In order to estimate in our experiments the accuracy and the stability constant of a given reconstructor  $\Psi$  we compute the empirical accuracy  $\hat{\eta}^{-1}$  and the empirical stability constant  $\hat{C}_{\Psi}^{\epsilon}$ , respectively defined as

$$\hat{\eta} = \sup_{x^{gt} \in \mathcal{S}} \|\Psi(Ax^{gt}) - x^{gt}\| \quad (5.2)$$

and

$$\hat{C}_{\Psi}^{\epsilon} = \sup_{x^{gt} \in \mathcal{S}} \frac{\|\Psi(Ax^{gt} + e) - x^{gt}\| - \hat{\eta}}{\|e\|} \quad (5.3)$$

where  $\mathcal{S} \subseteq \mathcal{X}$  is the test set and  $e$  is a noise realization from  $\mathcal{N}(0, \delta^2 I)$  with  $\|e\| \leq \epsilon$  (different for any datum  $x^{gt} \in \mathcal{S}$ ).

## 6 Numerical Results

In this section we report the results obtained from experiments A, B and C described in Section 5. In order to care about the stochasticity of our tests, we repeated  $T = 20$  times the experiments on the test sets, with different realizations of noise. In the following, we report the maximum value of the computed parameters  $\hat{\eta}$  and  $\hat{C}_{\Psi}^{\epsilon}$  over the T experiments.

### 6.1 Results of experiment A

Here we discuss the results obtained by the four models NN, ReNN, StNN, StReNN in experiment A, described in Section 5.2. Table 1 reports the mean values of the accuracy  $\hat{\eta}^{-1}$  and stability constant  $\hat{C}_{\Psi}^{\epsilon}$  computed on the test set. To graphically visualize the trade-off between accuracy and stability, we plot in Figure 3a  $\hat{C}_{\Psi}^{\epsilon}$  versus  $\hat{\eta}^{-1}$ . As expected, NN has excellent accuracy but it lacks in stability; on the contrary, ReNN appears as a good trade-off between accuracy and stability, since it shows a slightly higher value of  $\hat{\eta}^{-1}$  with respect to NN, whereas its constant  $\hat{C}_{\Psi}^{\epsilon}$  is dramatically lower (from a value greater than 32 in NN to about 10 in ReNN). With the introduction of a stabilizer, we observe that StNN and StReNN are  $\epsilon$ -stable since  $\hat{C}_{\Psi}^{\epsilon} < 1$ . Finally, by comparing the deep learning-based frameworks with the variational reconstructor  $\Psi_{\hat{K}}^{\lambda,L}$ , denoted as IS in the following, we observe that the proposed StNN and StReNN improve the IS accuracy while preserving the stability.

In Figure 3b we plot the reconstruction error:

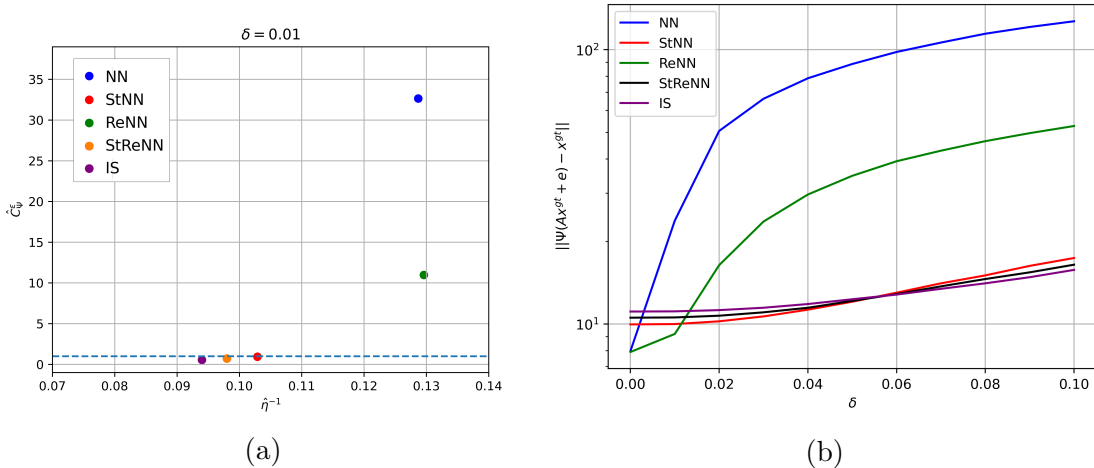
$$ERR = \|\Psi(Ax^{gt} + e) - x^{gt}\|$$

$\hat{\delta} = 0$	NN	StNN	ReNN	StReNN	IS
$\hat{\eta}^{-1}$	0.1287	0.1029	0.1296	0.0980	0.0940
$\hat{C}_{\Psi}^{\epsilon}(\delta = 0.01)$	32.6398	0.9269	10.9700	0.7046	0.5392

Table 1: Values of empirical accuracy and stability constant obtained in experiment A.

when the value of  $\delta$  varies in the interval  $[0, 0.1]$  for all the considered reconstructors. We observe that the errors of NN and ReNN methods increase very rapidly: for values of  $\delta$  near zero they are the lowest but they soon are overcome. Moreover, we emphasize that the stabilizer introduced in StNN and StReNN is very effective since the curves have a gentle slope with increasing  $\delta$ .

To show the statistical behavior over all the  $T=20$  tests, in Figure 4 we report the box plots of  $\hat{\eta}^{-1}$  and  $\hat{C}_{\Psi}^{\epsilon}$  (Figures 4a and 4b respectively). They show that the values lie in a very small range, except for very few exceptions, confirming the robustness of the proposed methods. Figure 5 shows an example of reconstruction with the different methods. The images confirm that NN amplifies the noise in the observed image, StNN stabilizes NN by reducing the noise, whereas ReNN and StReNN compute a more accurate reconstruction. We remark that ReNN and StReNN are both unsupervised tasks.

Figure 3: Results obtained in Experiment A. *Left.* Scatterplot of the stability constant versus the accuracy. *Right.* Plot of ERR versus  $\delta$ .

## 6.2 Results of experiment B

The results obtained in experiment B, described in Section 5.3, are reported in Table 2 and graphically shown in Figure 6. We remark that the difference between this experiment and the previous one is noise injection in the input of each network. Since this technique stabilizes the results, we have tested the methods with higher values of the noise variance ( $\delta = 0.075$  and  $\delta = 0.105$ ). In Figure 6a, we observe that the  $\hat{C}_{\Psi}^{\epsilon} < 1$  for all the reconstructors. Moreover, from the values of  $\hat{C}_{\Psi}^{\epsilon}$  reported in Table 2, it is evident that the stabilized

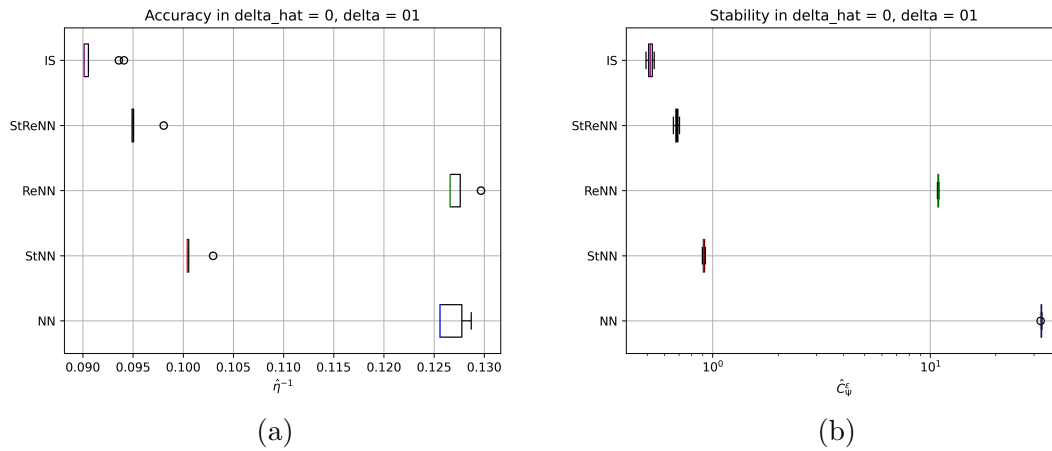


Figure 4: Boxplot of the results obtained in experiment A for accuracy (*Left*) and stability constant (*Right*) with  $T = 20$  executions.

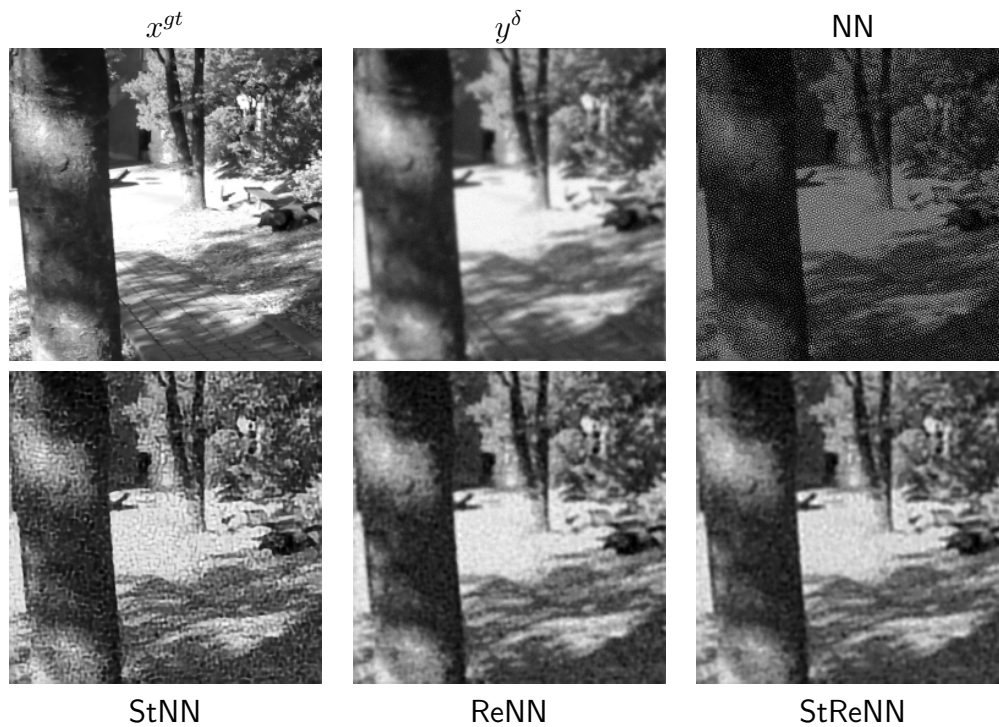
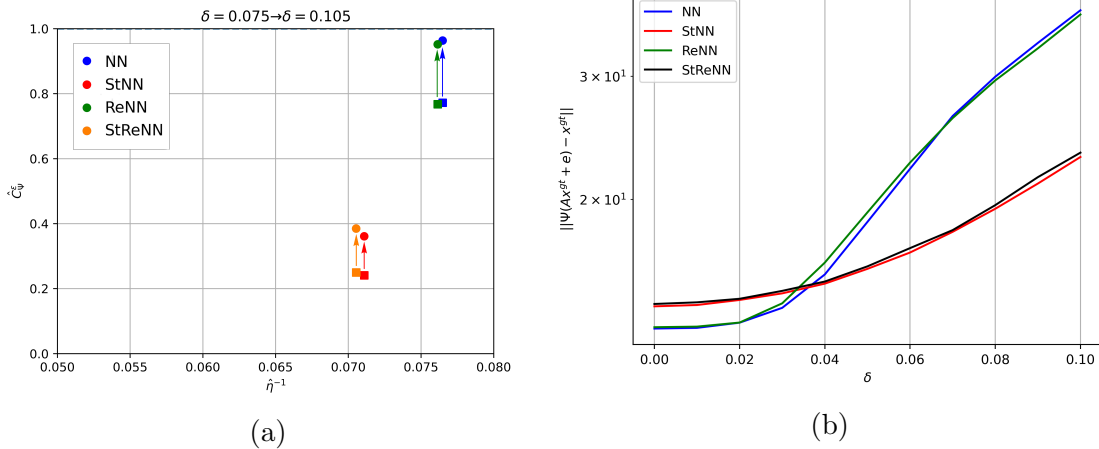


Figure 5: Example of reconstructions obtained by the NN, StNN, ReNN and StReNN methods on a test image of Experiment A.

$\delta^I = 0.025$	NN	StNN	ReNN	StReNN
$\hat{\eta}^{-1}$	0.0764	0.0710	0.0761	0.0705
$\hat{C}_{\Psi}^{\epsilon}(\delta = 0.075)$	0.7719	0.2408	0.7674	0.2495
$\hat{C}_{\Psi}^{\epsilon}(\delta = 0.105)$	0.9632	0.3608	0.9516	0.3846

Table 2: Values of empirical accuracy and stability constant obtained in experiment B.

reconstructors StNN and StReNN benefit a lot from noise injection. In Figure 6 we plot the reconstruction error for increasing noise variance  $\delta$  in  $[0, 0.025]$ . We observe that the error values of NN and ReNN methods are almost constant, proving that noise injection prevents instability (at least up to the noise level introduced as an input of the network). For values of  $\delta > 0.025$ , the curves relative to NN and ReNN grow rapidly, overtaking StNN and StReNN which show great stability versus high noise levels.

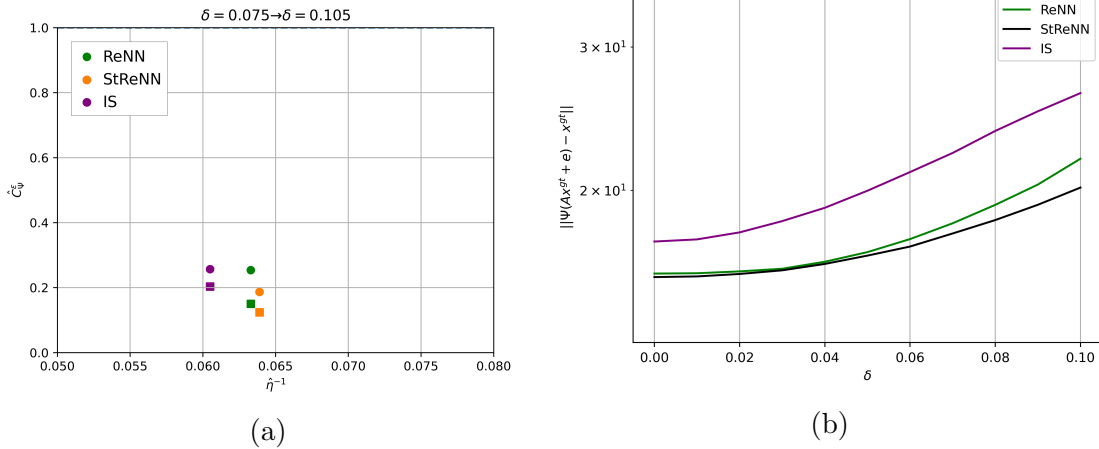
Figure 6: Results obtained in Experiment B. *Left.* Scatterplot of the stability constant versus the accuracy. *Right.* Plot of ERR versus  $\delta$ .

### 6.3 Results of experiment C

The results obtained in experiment C, described in Section 5.4, are reported in Table 3 and graphically shown in Figure 7. We remark that here we aim to experimentally verify Theorem 3.1 by showing that, if we train ReNN and StReNN as described in Section 5.4, their accuracy and stability constant are close to those of  $\Psi^{\lambda, L}$ . We test the reconstructors with  $\delta = 0.075$  and  $\delta = 0.105$ . Figure 7a shows that the markers relative to ReNN and StReNN are indeed close to the markers associated with IS. Table 3 confirms that the accuracy of ReNN and StReNN, as well as the stability constant of ReNN, well approximate those of IS. StReNN appears even more stable than IS, since its stability constant is lower than the one of IS by approximately 0.07. These results are confirmed by Figure 7.

$\hat{\delta} = 0.025$	ReNN	StReNN	IS
$\hat{\eta}^{-1}$	0.0633	0.0639	0.0605
$\hat{C}_{\Psi}^{\epsilon}(\delta = 0.075)$	0.1500	0.1238	0.2034
$\hat{C}_{\Psi}^{\epsilon}(\delta = 0.105)$	0.2536	0.1865	0.2566

Table 3: Values of empirical accuracy and stability constant obtained in experiment C.

Figure 7: Results obtained in Experiment C. *Left.* Scatterplot of the stability constant versus the accuracy. *Right.* Plot of ERR versus  $\delta$ .

## 7 Conclusions

After formalizing the concept of accuracy and stability of a reconstructor for the solution of discrete linear inverse problems, we have performed a theoretical analysis on neural network reconstructors. In particular, we proved in Theorem 2.1 that it is not possible to increase stability without decreasing accuracy, depending on a constant characterizing the solution process. Balancing the trade-off between stability and accuracy we have proposed new reconstructors: the ReNN approach increases the stability by inheriting, in the network training, regularization from a model-based scheme, the StNN framework stabilizes the solution process by reducing the impact of the noise on the input data performing few iterations of a model-based algorithm and, combining the two previous approaches, the StReNN scheme approximates the entire execution of a model-based iterative regularized solver. In the numerical experiments we compared our proposal with a standard neural network reconstructor, which exhibits high instability to noise perturbation on the data. The results show that our reconstructors improve the stability of neural networks by reducing its stability constant of around 92%, especially when stabilizers are introduced in StNN and StReNN, with minimal accuracy loss of about 10 – 20% (in one case we even gain accuracy with respect to neural networks). Our methods outperform end-to-end neural networks even when stabilization techniques such as noise injection are introduced. We believe that this new approach to solve noisy linear inverse problems with stable deep learning based tools is relevant in this field and it can be further theoretically extended to more general problems and applied to

the solution of real imaging applications.

## References

- [1] Ben Adcock and Nick Dexter. The gap between theory and practice in function approximation with deep neural networks. *SIAM Journal on Mathematics of Data Science*, 3(2):624–655, 2021.
- [2] Jaweria Amjad, Jure Sokolić, and Miguel RD Rodrigues. On deep learning for inverse problems. In *2018 26th European Signal Processing Conference (EUSIPCO)*, pages 1895–1899. IEEE, 2018.
- [3] Simon Arridge, Peter Maass, Ozan Öktem, and Carola-Bibiane Schönlieb. Solving inverse problems using data-driven models. *Acta Numerica*, 28:1–174, 2019.
- [4] Julius Berner, Philipp Grohs, Gitta Kutyniok, and Philipp Petersen. The modern mathematics of deep learning. *arXiv preprint arXiv:2105.04026*, 2021.
- [5] Mario Bertero, Patrizia Boccacci, and Christine De Mol. *Introduction to inverse problems in imaging*. CRC press, 2021.
- [6] Chris M Bishop. Training with noise is equivalent to tikhonov regularization. *Neural computation*, 7(1):108–116, 1995.
- [7] Pasquale Cascarano, Elena Loli Piccolomini, Elena Morotti, and Andrea Sebastiani. Plug-and-play gradient-based denoisers applied to ct image enhancement. *Applied Mathematics and Computation*, 422:126967, 2022.
- [8] Matthew J Colbrook, Vegard Antun, and Anders C Hansen. Can stable and accurate neural networks be computed?—on the barriers of deep learning and smale’s 18th problem. *arXiv preprint arXiv:2101.08286*, 2021.
- [9] Heinz W. Engl, Martin Hanke, and Andreas Neubauer. *Regularization of inverse problems*. 1996.
- [10] Heinz Werner Engl, Martin Hanke, and Andreas Neubauer. *Regularization of inverse problems*, volume 375. Springer Science & Business Media, 1996.
- [11] Davide Evangelista, Elena Morotti, and Elena Loli Piccolomini. rising: A new framework for model-based few-view ct image reconstruction with deep learning. *Computerized Medical Imaging and Graphics*, 103:102156, 2023.
- [12] Zalan Fabian, Reinhard Heckel, and Mahdi Soltanolkotabi. Data augmentation for deep learning based accelerated mri reconstruction with limited data. In *International Conference on Machine Learning*, pages 3057–3067. PMLR, 2021.
- [13] Martin Genzel, Jan Macdonald, and Maximilian Marz. Solving inverse problems with deep neural networks—robustness included. *IEEE Transactions on Pattern Analysis and Machine Intelligence*, 2022.

- [14] Nina M Gottschling, Vegard Antun, Ben Adcock, and Anders C Hansen. The troublesome kernel: why deep learning for inverse problems is typically unstable. *arXiv preprint arXiv:2001.01258*, 2020.
- [15] Harshit Gupta, Kyong Hwan Jin, Ha Q Nguyen, Michael T McCann, and Michael Unser. Cnn-based projected gradient descent for consistent ct image reconstruction. *IEEE transactions on medical imaging*, 37(6):1440–1453, 2018.
- [16] Per Christian Hansen. *Rank-deficient and discrete ill-posed problems: numerical aspects of linear inversion*. SIAM, 1998.
- [17] Per Christian Hansen. *Discrete inverse problems: insight and algorithms*. SIAM, 2010.
- [18] Per Christian Hansen, James G Nagy, and Dianne P O’leary. *Deblurring images: matrices, spectra, and filtering*. SIAM, 2006.
- [19] Yixing Huang, Alexander Preuhs, Günter Lauritsch, Michael Manhart, Xiaolin Huang, and Andreas Maier. Data consistent artifact reduction for limited angle tomography with deep learning prior. In *International workshop on machine learning for medical image reconstruction*, pages 101–112. Springer, 2019.
- [20] Chang Min Hyun, Seong Hyeon Baek, Mingyu Lee, Sung Min Lee, and Jin Keun Seo. Deep learning-based solvability of underdetermined inverse problems in medical imaging. *Medical Image Analysis*, 69:101967, 2021.
- [21] Elena Morotti, Davide Evangelista, and Elena Loli Piccolomini. A green prospective for learned post-processing in sparse-view tomographic reconstruction. *Journal of Imaging*, 7(8):139, 2021.
- [22] Jennifer L Mueller and Samuli Siltanen. *Linear and nonlinear inverse problems with practical applications*. SIAM, 2012.
- [23] Seungjun Nah, Tae Hyun Kim, and Kyoung Mu Lee. Deep multi-scale convolutional neural network for dynamic scene deblurring. In *CVPR*, 07 2017.
- [24] Daniel Obmann, Linh Nguyen, Johannes Schwab, and Markus Haltmeier. Augmented nett regularization of inverse problems. *Journal of Physics Communications*, 5(10):105002, 2021.
- [25] Allan Pinkus. Approximation theory of the mlp model in neural networks. *Acta numerica*, 8:143–195, 1999.
- [26] Olaf Ronneberger, Philipp Fischer, and Thomas Brox. U-net: Convolutional networks for biomedical image segmentation. In *International Conference on Medical image computing and computer-assisted intervention*, pages 234–241. Springer, 2015.
- [27] Otmar Scherzer, Markus Grasmair, Harald Grossauer, Markus Haltmeier, and Frank Lenzen. Variational methods in imaging. 2009.

- [28] Andrei Nikolaevich Tikhonov, AV Goncharky, VV Stepanov, and Anatoly G Yagola. *Numerical methods for the solution of ill-posed problems*, volume 328. Springer Science & Business Media, 1995.
- [29] Weiwen Wu, Dianlin Hu, Wenxiang Cong, Hongming Shan, Shaoyu Wang, Chuang Niu, Pingkun Yan, Hengyong Yu, Varut Vardhanabhuti, and Ge Wang. Stabilizing deep tomographic reconstruction: Part a. hybrid framework and experimental results. *Patterns*, 3(5):100474, 2022.
- [30] Weiwen Wu, Dianlin Hu, Wenxiang Cong, Hongming Shan, Shaoyu Wang, Chuang Niu, Pingkun Yan, Hengyong Yu, Varut Vardhanabhuti, and Ge Wang. Stabilizing deep tomographic reconstruction: Part b. convergence analysis and adversarial attacks. *Patterns*, 3(5):100475, 2022.
- [31] Zhengxia Zou, Tianyang Shi, Zhenwei Shi, and Jieping Ye. Adversarial training for solving inverse problems in image processing. *IEEE Transactions on Image Processing*, 30:2513–2525, 2021.

## A Estimation of Local Lipschitz Constant

We state in the following Theorem a lower bound for the Lipschitz constant  $L^\epsilon(\Psi, Ax)$ .

**Theorem A.1.** If  $\Psi : \mathbb{R}^m \rightarrow \mathbb{R}^n$  is an  $\eta^{-1}$ -accurate reconstructor,  $x, x' \in \mathcal{X}$  such that  $\|A(x - x')\| < \eta$ , then for any  $\epsilon \geq \eta$ , it holds

$$L^\epsilon(\Psi, Ax) \geq \frac{\|x - x'\| - 2\eta}{\epsilon}. \quad (\text{A.1})$$

*Proof.* Let  $y = Ax$ . By the definition of  $\epsilon$ -Lipschitz constant we have

$$L^\epsilon(\Psi, y) = \sup_{z: \|z-y\| \leq \epsilon} \frac{\|\Psi(z) - \Psi(y)\|}{\|z - y\|}$$

Since, by hypothesis,  $\|Ax - Ax'\| = \|A(x - x')\| < \eta \leq \epsilon$ , we have:

$$\begin{aligned} L^\epsilon(\Psi, y) &= \sup_{z: \|z-y\| \leq \epsilon} \frac{\|\Psi(z) - \Psi(y)\|}{\|z - y\|} \geq \frac{\|\Psi(Ax') - \Psi(Ax)\|}{\|A(x' - x)\|} \\ &= \frac{\|\Psi(Ax') - x' - \Psi(Ax) + x + x' - x\|}{\|A(x' - x)\|} \\ &\geq \frac{-\|\Psi(Ax') - x'\| - \|\Psi(Ax) - x\| + \|x' - x\|}{\|A(x' - x)\|} \\ &> \frac{\|x' - x\| - 2\eta}{\eta} \stackrel{(\eta \leq \epsilon)}{\geq} \frac{\|x' - x\| - 2\eta}{\epsilon} \end{aligned}$$

which implies that

$$L^\epsilon(\Psi, y) > \frac{\|x' - x\| - 2\eta}{\epsilon}.$$

■

Consequently, a sufficient condition that implies instability is that there exists  $x, x' \in \mathcal{X}$  such that  $\|A(x - x')\| < \eta \leq \epsilon$  and

$$\begin{aligned} \frac{\|x - x'\| - 2\eta}{\epsilon} &\geq 1 \iff \\ \|x - x'\| &\geq \epsilon + 2\eta \end{aligned} \tag{A.2}$$

This way, we moved the problem of proving instability of  $\Psi$  to a problem of finding points  $x, x' \in \mathcal{X}$  distant from each other such that their difference lies close to the kernel of  $A$ . In the following, we will prove that this condition is closely related to the conditioning of  $A$  and, in particular, to how quick their singular values decay.

**Theorem A.2.** Let  $x^{gt} \in \mathcal{X}$  and  $y = Ax^{gt}$ . Let  $(\sigma_1, \dots, \sigma_n)^T$  be the singular values of  $A$  and  $(v_1, \dots, v_n)^T$  the left-singular vectors associated to  $(\sigma_1, \dots, \sigma_n)^T$ . For any  $r = 1, \dots, n$ , define  $V_r := \text{Span}\{v_r, v_{r+1}, \dots, v_n\}$  the subspace defined by the left singular vectors of  $A$  associated with singular values less than or equal to  $\sigma_r$ . Consider the accuracy  $\eta^{-1} > 0$  to be fixed. Let  $t < n$  be a positive integer and  $\eta > 0$ . Then there are points  $x, x' \in \mathcal{X}$  such that  $\|x - x'\| = \frac{\eta}{\sigma_t}$  but  $\|A(x - x')\| < \eta$ . In particular, for every  $x \in \mathcal{X}$ , the set of such points defines a vector space of dimension  $n - t$ .

*Proof.* Let  $t < n$  be fixed. Consider  $x \in \mathcal{X}$ ,  $\delta x \in V_{t+1}$  and  $x' := x + \delta x$ .

Since  $\delta x \in V_{t+1}$ , then we can write it in coordinates with respect to the basis  $\{v_{t+1}, \dots, v_n\}$  of  $V_{t+1}$ , i.e.,

$$\delta x = \sum_{i=t+1}^n a_i v_i.$$

Since the  $V$  matrix of the SVD decomposition of  $A$  is an orthogonal matrix, its columns  $\{v_1, \dots, v_n\}$  forms an orthonormal base of  $\mathbb{R}^n$ . Thus

$$\|x - x'\| = \|\delta x\| = \sqrt{\sum_{i=t+1}^n a_i^2}$$

and

$$\|A(x' - x)\| = \|A\delta x\| = \|U\Sigma V^T \delta x\|$$

but

$$U\Sigma V^T \delta x = \sum_{i=1}^n \sigma_i (v_i^T \delta x) u_i = \sum_{i=1}^n \sigma_i \left( v_i^T \sum_{j=t+1}^n a_j v_j \right) u_i = \sum_{i=t+1}^n \sigma_i a_i u_i$$

which implies that

$$\|A(x - x')\| = \sqrt{\sum_{i=t+1}^n \sigma_i^2 a_i^2} \leq \sqrt{\sum_{i=t+1}^n \sigma_t^2 a_i^2} = \sigma_t \sqrt{\sum_{i=t+1}^n a_i^2} = \sigma_t \|\delta x\|$$

As a consequence, if we choose  $\|\delta x\|$  to be  $\|\delta x\| = \frac{\eta}{\sigma_t}$  we have that:

$$\begin{aligned} \|A(x - x')\| &< \eta \\ \|x - x'\| &= \|\delta x\| = \frac{\eta}{\sigma_t} \end{aligned}$$

■

In particular, given an  $\eta^{-1}$ -accurate reconstructor  $\Psi$ , we can find  $x, x' \in \mathcal{X}$  such that  $\|A(x - x')\| < \eta$  and  $\|x - x'\| = \frac{\eta}{\sigma_t}$  where  $t$  is a positive integer such that  $t < n$ . Consequently, joining Theorem A.1 and Theorem A.2, we have

$$L^\epsilon(\Psi, \tilde{y}) \geq \frac{1}{\epsilon} \left( \|x - x'\| - 2\eta \right) = \frac{1}{\epsilon} \left( \frac{\eta}{\sigma_t} - 2\eta \right) = \frac{1}{\epsilon} \left( \frac{\eta - 2\sigma_t\eta}{\sigma_t} \right) \quad (\text{A.3})$$

which shows that any  $\eta^{-1}$ -accurate reconstructor  $\Psi$  is unstable as soon as

$$\begin{aligned} \frac{1}{\epsilon} \left( \frac{\eta - 2\sigma_t\eta}{\sigma_t} \right) &\geq 1 \iff \\ \sigma_t &\leq \frac{\eta}{\epsilon + 2\eta} \end{aligned} \quad (\text{A.4})$$

Moreover, Theorem A.2 shows that given  $x \in \mathcal{X}$  and  $y = Ax$ , the set of points  $x'$  such that  $\|A(x - x')\| < \eta$  with distance  $\frac{\eta}{\sigma_t}$  from  $x$  has dimension  $n - t$  which implies that, if the smallest  $t$  such that (A.4) is low, the probability of getting a locally unstable point  $x'$  is high.

## B Neural Network Details

The network used in our experiments is a slight modification of the original U-Net [26] architecture, already used in [21, 11], whose diagram is shown in Figure 8.

Each network is trained for 50 epochs with the Adam optimization algorithm and fixed step size of  $10^{-4}$ . The network is trained to minimize the Mean Squared Error (MSE) between the output and the processed input, for each dataset, with no additional modifications such as regularizers or the use of Dropout layers. The batch size is set to the maximum value our GPU could handle, that is 8. The training is executed on an NVIDIA RTX A4000 GPU card, requiring approximately 1 to 2 hours to be completed.

